REVIEW

Check for updates

Steam reforming of methane: state of the art and novel technologies

Aimaro Sanna, [iD][a] Dillon Openshaw,[b]
Princess Oghotomo[c] and Giuseppe Bagnato [iD] *[b]

Steam methane reforming (SMR) is one of the most promising technologies for sustainable hydrogen production. Although numerous reviews have been published on the catalysts developed for SMR, this field is advancing rapidly, prompting this review to focus on recent developments in new promoters, supports, and structural improvements for SMR catalysts. These advancements aim to reduce carbon deposition and sintering while enhancing catalyst activity and stability. This review provides a comprehensive analysis of recent research focusing on improving SMR processes using various catalyst types and operating conditions, as well as examining emerging SMR technologies. Additionally, key challenges related to SMR catalysts are discussed, along with recent progress in conventional SMR using Ni-based, transition metal, and noble metal catalysts, and advancements in SMR processes. The recent literature has highlighted the utility of supported bi-metallic catalysts and advanced SMR technologies, including chemical looping, sorption enhancement, and membrane reactors, in commercialising SMR technologies.

1. Introduction

Increased greenhouse gas emissions, from fossil fuel usage and industrial processes, are recognised as one of the main causes of climate change.[1] Despite the adoption of the Kyoto Agreement in 1997 and the Paris Agreement in 2016, the rate of CO_2 emissions has increased steadily until 2020, when there was a 7% decrease in emissions, due to a shift from fossil fuels to renewable energy and a reduced use of energy due to COVID pandemic restrictions.[2]

H_2 is an energy carrier that is recognized as a potential alternative to fossil fuels, due to its high energy density[3] and carbon free utilization.[4] Considerable amounts of recent research have focused on developing sustainable H_2 production technologies,[5] such as reforming, gasification, fermentation, and electrolysis. Today, H_2 is widely produced through steam reforming of natural gas (SRNG) due to its low cost.[6] However, SRNG releases CO_2 into the atmosphere and is reliant on a non-renewable feedstock, making it an unsustainable process.[7]

Natural gas is predominantly composed of methane[8] which is converted into H_2 *via* the steam methane reforming (SMR – eqn (1)) and water gas shift (WGS – eqn (2)) reactions.[9] A more sustainable source of methane is biogas which is produced *via* anaerobic digestion of biomass.[10]

[a] *Heriot-Watt University, Edinburgh, EH14 4AS, UK*

[b] *KORE group, Lancaster University, Lancaster, LA1 4YW, UK.*
 E-mail: g.bagnato@lancaster.ac.uk

[c] *Teesside University, Middlesbrough, TS1 3BX, UK*

Biomass refers to any non-fossilised organic material (food crops, wood, algae, waste *etc.*)[11] and is considered a sustainable feedstock as it is renewable and carbon neutral.[12]

As shown in Fig. 1, in a conventional NGSR process, natural gas is first desulfurized to avoid catalyst deactivation. The natural gas is then sent to the reforming unit where steam is introduced, and the reforming process takes place.
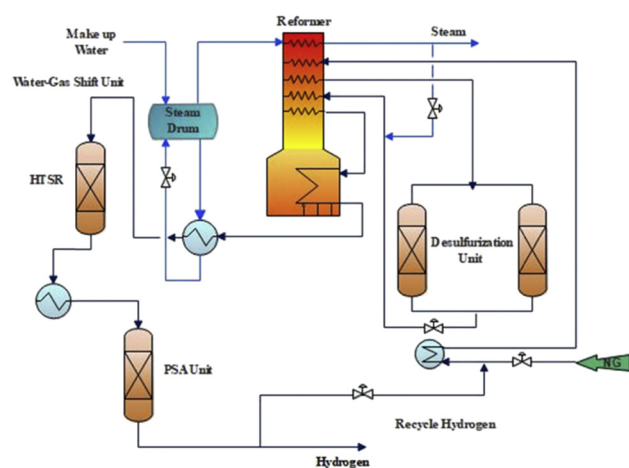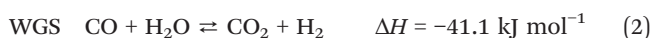
$$\text{SMR} \quad CH_4 + H_2O \rightleftharpoons CO + 3H_2 \qquad \Delta H = +206.1 \text{ kJ mol}^{-1} \quad (1)$$

$$\text{WGS} \quad CO + H_2O \rightleftharpoons CO_2 + H_2 \qquad \Delta H = -41.1 \text{ kJ mol}^{-1} \quad (2)$$

Fig. 1 A flow diagram of industrial H_2 production using a conventional natural gas steam reforming process.[13]

This journal is © The Royal Society of Chemistry 2025

React. Chem. Eng., 2025, **10**, 1963–1977 | 1963

$$CH_4 + 2H_2O \rightleftharpoons CO_2 + 4H_2 \qquad \Delta H = +165 \text{ kJ mol}^{-1} \qquad (3)$$

The SMR reaction is highly endothermic requiring a temperature of 800 °C to maximise methane conversion. The stream in the reformer output (syngas) is sent to the WGS reactor, where steam is added to syngas to convert CO into H_2.[14] The H_2 produced is then purified using pressure swing adsorption.[15]

Industrial catalysis has been a crucial factor in the success of the petrochemical and fertiliser sectors, and its importance is paramount to the development of commercially viable SMR technologies.[16] Ni catalysts are commonly used in SMR processes due to their high activity and lower cost relative to noble metals.[17] However, a major challenge facing Ni catalysts is deactivation. The most common mechanisms of SMR catalyst deactivation are sintering, metal oxidation, thermal degradation of supports, and coke formation.[18]

Coking is the build-up of carbon deposits on the catalyst surface, blocking active sites and/or pores causing activity loss. Ginsburg *et al.*[19] stated that there are five types of coke formation found on Ni catalysts: atomic carbon (C_α), polymeric films/filaments (C_β), vermicular whiskers/fibres (C_v), Ni carbide (C_γ), and graphitic platelets (C_c). Fig. 2 summarises the mechanism of coke formation. Atomic carbon (C_α) and polymeric films/filaments (C_β) are formed at low temperatures, but are then converted to graphitic platelets/films (C_c) and vermicular whiskers/fibres (C_v) at high temperatures.[20] Coke formation on Ni catalysts can be reduced during SMR by supporting the catalyst with metal oxides (Al_2O_3, CeO_2, MgO) and metal promoters such as noble metals (Ru, Rh, Pt).[21]

Sintering occurs when there is growth of metal crystallites in the catalyst causing loss of active surface area of the support.[21] There are several mechanisms of sintering including crystallite migration, atom migration, spreading/splitting, and transport of vapour. Fig. 3 depicts atom and crystallite migration mechanisms. During crystallite migration, the crystallite moves over the surface and grows to form large crystallites that combine with other crystals. The same process occurs during atomic migration but in this case, atoms migrate from crystallites and combine with larger crystals.[22] Temperature, atmosphere, support type, promoters, metal and pore size all affect the sintering rate.[20] Sintering can be mitigated using high melting point catalyst supports[23–25] or the use of other metals as promoters.[26,27]
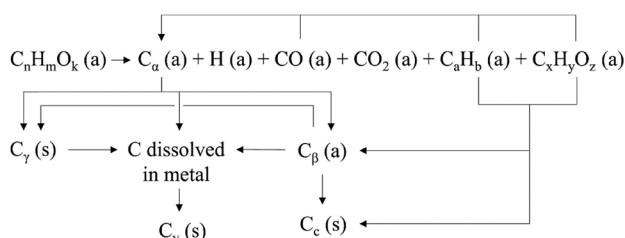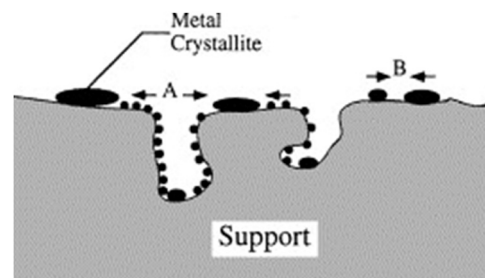

Fig. 3 Sintering mechanism of crystallite migration (A) and atom migration (B).[28]

Several advanced technologies have also been developed to improve the commercial viability of SMR such as sorbent-enhanced SMR, oxidative SMR, chemical looping process, photocatalytic SMR, thermo-photo hybrid SMR, solid oxide fuel cells (SOFCs), plasma SMR, and electro-catalytic SMR and membrane reactors for SMR. The aim of this review is to provide the reader with an understanding of the concepts underpinning SMR technologies, the challenges associated with the development of technologies, and an overview of how recent literature has addressed these challenges to commercialise H_2 production from SMR.

2. Ni based catalysts

Ni-based catalysts are mostly used in the SMR process because of their low cost, high activity, and H_2 selectivity, although they are prone to deactivation *via* coking and sintering. To prevent this, noble metal promoters (such as Ru, Rh, and Pt), non-noble metals (such as Co, Cu, and Mo), perovskite oxides, metal oxides, and supports (Al_2O_3, CeO_2, SiO_2, ZrO_2, MgO, and $MgAl_2O_4$) are added.[7,29]

2.1. Promoters

There are different types of promoters for Ni-based catalysts in SMR such as those based on metal–metal interactions, redox metal oxide promoters, and non-metal promotors.[5]

The introduction of a second metal to a Ni-based catalyst as a promoter can improve its activity and selectivity. For example, adding Fe to Ni forms a Ni–Fe alloy, which achieves a high methane conversion (up to 97.5% at 900 °C).[7] The most common promoters for Ni-based catalysts are noble metals (*e.g.* Ru, Rh, Pt, Ir, Ag, and Au) and rare earth metals (*e.g.* Ce and Nb).

Noble metals such as Rh, Ir, Pt and Ru have also been investigated as promoters in Ni/Al_2O_3. Morales-Cano *et al.*[26] studied and compared the results of using Rh, Ir and Ru as promoters in Ni/Al_2O_3 and concluded that the formation of Ni–Rh and Ni–Ir alloys prevented sintering as a result of the mobility of the Ni species into the metals, although at a temperature of 800 °C and pressure of 22 bar, the catalyst was subjected to deactivation. The Ni–Ru alloy exhibited poor sintering resistance due to its low mobility. The effect of Pt in a $Ni/MgAl_2O_4$ catalyst was investigated across a range of 0.01 to 1.0 wt%. At 1.0 wt%, the Ni–Pt species were fully

Fig. 2 Mechanism of coke deposition.[18]

1964 | *React. Chem. Eng.*, 2025, **10**, 1963–1977

This journal is © The Royal Society of Chemistry 2025

dispersed on the catalyst surface, leading to the best catalytic activity and stability. However, as the Pt content decreased so did the catalyst's activity.[24]

Ag and Au have both been tested as promotors for Ni-based catalysts to reduce coke formation.[30,31] Ag and Au were proposed as promoters for Ni catalysts in a temperature range of 450 °C to 700 °C and a C/S ratio of 1 : 4. As shown in Fig. 4, adding Au at temperatures lower than 600 °C enhanced the catalytic activity and stability of Ni/Al$_2$O$_3$. In contrast, adding Ag decreased the catalytic properties of Ni/Al$_2$O$_3$.[32]

Ceria (Ce) has also been used as a promoter, improving catalytic performance and reducing coke formation, thus increasing catalyst activity and stability.[33] Ni–Ce/Mg–Al showed high activity at low temperatures (175 °C) achieving a methane conversion of 54%.[34] Furthermore, a Ce content of 1.02 wt% in a Ni–Ce/Al catalyst exhibited a methane conversion of 75% and high coking resistance using a S/C ratio of 3.[34,35]

Niobium (Nb) is an excellent promoter that helps increase the surface area of the catalyst for methane and carbon adsorption. A Ni–Co/Al$_2$O$_3$–MgO/Nb–Zr catalyst exhibited a high methane conversion of 86.96% and CO$_2$ selectivity of 87.84%.[36] The addition of Nb in the Ni/Ce–Al$_2$O$_3$ catalyst reduced carbon deposition on the catalyst and sintering by controlling the Ni particle size dispersion and acidity of the catalyst.[37]

Different oxides such as MgO, CaO, and La$_2$O$_3$ have been investigated as promoters to enhance Ni-based catalysts' performance and coking resistance. MgO, CaO, and La$_2$O$_3$ were applied as promoters for Ni–Ce$_{0.8}$Zr$_{0.2}$O$_2$ catalysts. Among these, La$_2$O$_3$ exhibited a higher catalytic activity and stability, achieving a methane conversion of 47.4%, at 600 °C and a H$_2$/CO ratio of 6.8.[39] The addition of MgO as a promoter to Ni/SBA-15 improved catalyst performance. Over 620 hours at 850 °C, methane conversion decreased from 98% to 85%, while CO$_2$ selectivity dropped from 92% to around 77%. MgO played a key role in enhancing the dispersion of Ni species and promoting CO$_2$ adsorption, which helped suppress carbon deposition.[40] When Ni

catalysts were promoted by CuO, ZnO, Ga$_2$O$_3$, or Gd$_2$O$_3$, the latter proved to be the best promoter exhibiting a H$_2$ yield of 87% and methane conversion of 83% with a H$_2$/CO ratio of ~1.0.[40] The MgO promoter for the Ni–Ce$_{0.8}$Zr$_{0.2}$O$_2$ catalyst exhibited excellent catalyst performance, resulting in a methane conversion of 95% at a temperature of 800 °C for 200 h as a result of its high Ni dispersion, crystallite size, and catalyst surface area.[41]

Boron is the only known non-metal promoter currently investigated for Ni-based catalysts.[5] Boron as a promoter is known to make Ni-based catalysts coke resistant by covering the subsurface sites and preventing the diffusion of carbon into the bulk.[42] Boron has been shown to improve catalyst activity and reduced coke formation by 80%. The inclusion of boron improved methane conversion from 56% to 61% in a system utilising a Ni catalyst at 800 °C and 1 atm.[43]

2.2. Ni-based solid solution catalysts

MgO improves the H$_2$ concentration in the product syngas by inhibiting the desorption of CO from the catalysts surface. NiO and MgO form a solid solution which enhances the dispersion of Ni particles, improving the catalyst's activity and stability.[44] 10 wt% Ni supported on NiO–MgO (solid solution) exhibited a high catalyst activity and no carbon deposition at 700 °C.[45] The solid-solution catalyst for CO$_2$ reforming of methane achieved a methane conversion of 91% at an S/C ratio of 1, atmospheric pressure, and 790 °C.[44] While the NiO–MgO solid solution is not ideal for SMR, its performance can be improved by stabilizing the MgO and optimizing factors such as Ni loading and the S/C ratio. Additionally, thermally treating the NiO–MgO solid solution can enhance its effectiveness.[45]

2.3. Physical–chemical characteristics of supports

2.3.1. Ni particle size. It is known that particle size reduction significantly affects the activity of SMR catalysts and hinders coke formation, due to the increased surface-to-volume ratio.[46–48] Pashchenko et al.[49] demonstrated this using a validated CFD model that calculated the effectiveness factor of Ni/Al$_2$O$_3$ catalysts at particle diameters between 0.5 and 4 mm. The effectiveness factor accounts for intraparticle diffusion of reactants into the catalyst particle. The higher the effectiveness factor, the less the catalyst's activity was being reduced by diffusion limitations. The reactions were modelled at 630 and 930 °C and a S/C ratio of 3. At both temperatures, the effectiveness factor increased exponentially as particle diameter reduced. Ni particle size can be controlled by the calcination and reduction temperature and the extent of Ni loading in the catalyst.[50,51] Bej et al.[51] observed this using an alumina supported NiO–SiO$_2$ catalyst, where the crystallite size of NiO was in the range of 9–15 nm, Ni loading ranged between 5 and 15% and the calcination temperature was in the range of 350–500 °C. The optimum conditions of the steam reforming reaction were a temperature of 700 °C with a S/C ratio of 3.5 resulting in a
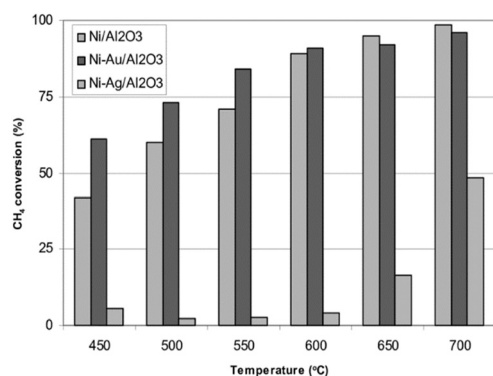

Fig. 4 Methane conversion over Au and Ag as promoters for Ni catalysts vs. temperature.[38]

This journal is © The Royal Society of Chemistry 2025

React. Chem. Eng., 2025, **10**, 1963–1977 | **1965**

methane conversion of 95.7%. The calcination reduced the size of the Ni nanoparticles and increased the Ni dispersion. 700 °C was observed to be the optimal temperature for SMR due to the formation of Ni aluminate.[52]

2.3.2. Support morphology. The surface morphology of a catalyst greatly effects its SMR activity. Egg shell catalysts are characterised by the active components' dispersion in the outer region (shell) of the catalyst, improving the percentage of active sites used to catalyse the process.[53–55] Cho et al.[56] compared the effectiveness of Ni on tube-shaped $MgAl_2O_4$ pellets using a homo-type and egg shell distribution (Fig. 5). The results demonstrated that the egg-shell-type (3.5 wt% Ni) catalyst had a higher activity and coke resistance than the homo-type (5 wt% Ni) at a S/C of 0.5.

Cho et al.[54] also tested egg-shell-type and homo-type catalysts, prepared with Ni and/or ruthenium placed on the outer (shell) and inner regions of alumina pellets. The egg-shell-type 1 wt% Ru/Al_2O_3 catalyst demonstrated higher methane conversion compared to the homo-type 1 wt% Ru/Al_2O_3 catalyst. Additionally, the egg-shell-type bimetallic catalyst (5 wt% Ni/0.7 wt% Ru) exhibited an even greater methane conversion than the egg-shell-type Ru catalyst alone. This was likely due to the enhanced accessibility of active sites on the outer surface of the catalyst and the synergistic effect between Ni and Ru.

Among the core/shell structures (homo-type catalysts), the first two exhibited the best performance at 750 °C and a H_2O/CH_4 ratio of 2, achieving a methane conversion of 97%, due to enhanced stability and active site accessibility provided by the core–shell structure. The presence of Mg contributed to improved resistance to coke formation. Additionally, the yolk–shell structure of Ni@HSS (hollow silica spheres) showed outstanding performance for 55 hours, with no detectable carbon deposition, due to the unique architecture of hollow spheres, which enables better diffusion of reactants, more effective exposure of active sites, and enhanced resistance to carbon deposition.[57]

The robust bimetallic Ni–La@KCC-1 catalyst exhibited a high methane and CO_2 conversion of 92% and 88%, respectively, for over 72 h at 750 °C and a high H_2/CO ratio with a small amount of carbon deposition being observed.[58]

Fig. 5 Schematic diagram of egg-shell-type and homo-type catalysts with the coke formation mechanism.[56]

The pore structure of a catalyst plays a crucial role in its performance, as demonstrated by the preparation of monomodal $Ni–SiO_2–NH_3 \cdot H_2O$, bimodal $Ni–SiO_2–urea$, and non-porous $Ni–SiO_2–NaOH$ catalysts for methane reforming. The bimodal Ni catalyst, which had the largest surface area, exhibited higher catalytic activity and stability, while the non-porous $Ni–SiO_2–NaOH$ catalyst showed lower activity due to its reduced surface area.[59] Other morphologies of Ni-based catalysts are shown in Fig. 6.

2.4. Novel metal oxide substrates

Various researchers have investigated different metal oxide substrates such as spinel ABO_4 and A_2BO_4 (Ni/La_2O_3), perovskites ABO_3 ($Ni–Al_2O_3$), hexaaluminates $AB_yAl_{12-y}O_{19-\delta}$ (hexaaluminates $LaNi_yAl_{12-y}O_{19-\delta}$) and solid solutions (NiO–MgO) as supports to get excellent catalyst performance.[60]

Ni catalysts are typically supported on metal oxides such as ZrO_2, CeO_2, K_2O, and MgO, which are used as promoters. Chawl et al.[61] investigated the production of syngas via CO_2 reforming of methane over Ni-based perovskite catalysts. They found that when 10 wt% Ni was supported on Al_2O_3 with promoters such as ZrO_2, CeO_2, K_2O, and MgO, the catalysts exhibited higher activity, stability, and long-term performance compared to un-promoted catalysts. They concluded that ZrO_2 improved metal particle dispersion on the catalyst surface.

Perovskite-type oxides such as $CaTiO_3$, $SrTiO_3$, $BaTiO_3$, and $LaAlO_3$ are commonly used as promoters for Ni-based catalysts in SMR. While perovskite oxides enhance the performance of Ni catalysts compared to unsupported Ni/Al_2O_3, $Ni/LaAlO_3$ stands out as the most active catalyst, effectively suppressing carbon formation.[62,63]

Other complex crystal oxide supports, such as hexaaluminates ($LaNi_xAl_{12-x}O_{19-\delta}$), have also shown excellent catalytic performance and low coke formation at high temperatures. Among them, hexaaluminates with $LaNi_xAl_{12-x}O_{19-\delta}$ (where x = 1.0 and 0.9) exhibited methane and CO_2 conversions of 97.4% and 98%, respectively.[64]

In the case of $Ni/Ce_{0.95}M_{0.05}O_{2-\delta}$ (M = Zr, Pr, La), Ni supported on Zr-doped ceria showed the highest surface area. When tested at three temperatures (600 °C, 750 °C, and 900 °C), increasing the vapour/CH_4 ratio at 600 °C resulted in high H_2 yield and limited coke formation. At 750 °C, the catalyst achieved the highest methane conversion.[65]

2.5. Self-supported Ni catalysts

Self-supported Ni catalysts with structured carrier shapes exhibited excellent SMR catalyst performance. An example of this is a honeycomb-type Ni catalyst, which has been found to achieve 95% methane conversion at an S/C ratio of 1.362. This was linked to steam treatment and H_2 reduction at 1173 K, forming more Ni fine particles at the surface.[66] However, a Ni honeycomb catalyst with a density of 2300 cells per square inch (cpsi) exhibited a much higher catalyst activity compared to that of a Ni honeycomb catalyst with a cell
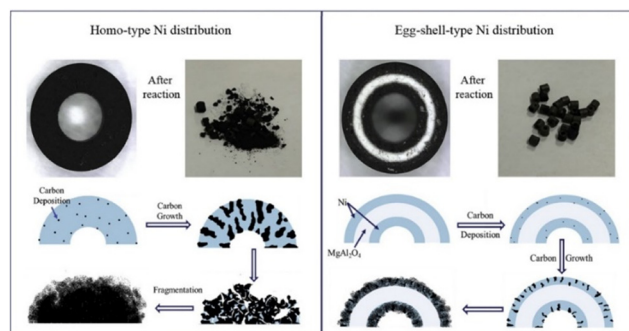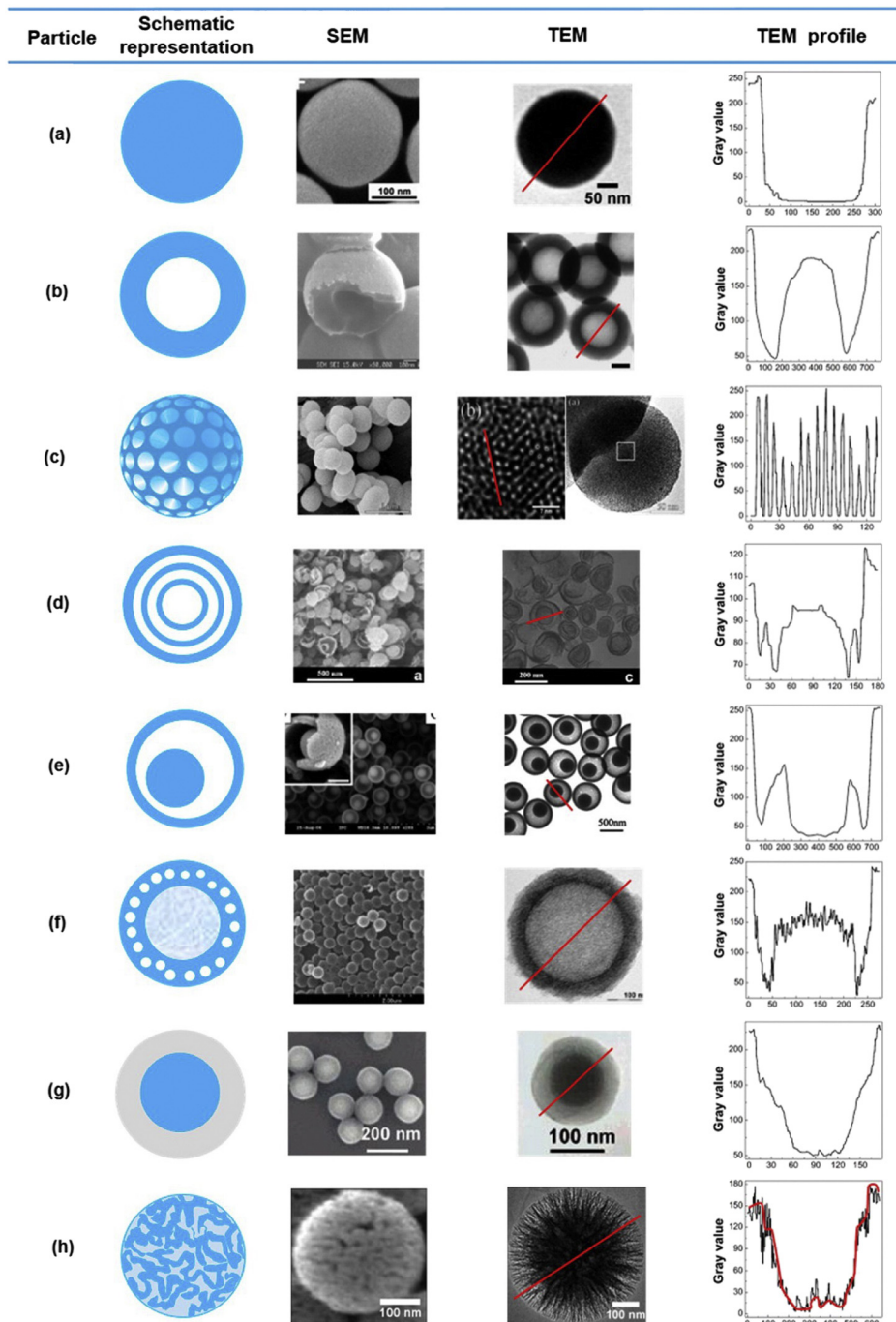
1966 | React. Chem. Eng., 2025, **10**, 1963–1977

This journal is © The Royal Society of Chemistry 2025

Fig. 6 (a) Nonporous,[68] (b) hollow,[69] (c) ordered mesoporous,[70] (d) multi-shell,[71] (e) yolk–shell,[57] (f) hollow with hierarchical pores,[60] (g) core–shell[72] and (h) KCC-1.[73]

density of 700 cpsi at an S/C ratio of 1.36 and in a temperature range of 873–1173 K, which shows the direct relation between catalyst activity and increased geometric surface area.[66]

A Ni coil catalyst achieved a high geometric surface area of 88.1 cm^2 cm^{-3} at an S/C ratio of 0.62–2.48 and a temperature of 1073 K. This resulted in a methane conversion of 94.0%, CO selectivity of 91.1%, and CO$_2$ selectivity of 8.9%.[67] Additionally, the introduction of

metallic foam improved methane conversion by 29.5% and the rate of H$_2$ production by 47.6%.[67]

3. Other non-noble metal catalysts

3.1. Cobalt-based catalysts

The microkinetic analysis of Co based catalysts showed that the dominant reaction path is like that of Ni catalysts.

There are two dominant reaction pathways on the Co catalyst for the formation of CO, namely C + O and CH + O paths as shown in Fig. 7. In the C + O path, methane is dehydrogenated to C* which then pairs with O* to form CO_2, while in the CH + O path, CH* pairs with O* to form CHO*.[7]

Coke formation comes after the surface reaction pathway mechanism, where the C* species dissolves into the metal bulk forming carbides and then migrates to the larger particles to form a carbon deposit.[7]

Co-based catalysts show satisfactory performance at low cost. Coke formation and metal oxidation under operating conditions lead to Co deactivation, but this can be prevented using different promoters (noble metals), supporters (earth metal oxides like MgO, SrO, CaO, or BaO and other metal oxides like TiO_2 or SiO_2) or adding another metal to form a bimetallic catalyst.[74] The use of promoters like noble metals improves the performance of the Co catalyst. For example, low concentration (0.03–0.43 wt%) of Pt-promoted Co/Al_2O_3 catalysts results in high catalyst activity and selectivity in comparison to Co/Al_2O_3 without a promoter and increasing the Pt content to 0.43 wt% also slightly improves the catalytic activity.[74,75] Co can be supported on earth metal oxides like MgO, SrO, CaO, or BaO, and other metal oxides like Al_2O_3 or SiO_2. Amongst these, MgO exhibited the highest catalyst activity and stability with a methane conversion of 94%, CO yield of 93%, H_2 yield of 90% and H_2/CO ratio of 0.97.[76] Alumina-supported NiCo bimetallic catalysts achieved a methane conversion of 75% and high selectivity[77] at 700 °C and a S/C ratio of 1. In investigating the performance of Co and bimetallic Co-based SMR catalysts (Co, Co–Ni, Co–Cu, and Co–Al) supported on CeO_2, results show that Co–Ni exhibits the best catalyst performance achieving a methane conversion of 76.1%, 58.5% H_2 selectivity and 44.5% H_2 yield.[78] This is due to Ni's well-known activity in breaking C–H bonds and synergistic activity when combined as an alloy with Co (Co–Ni), with the latter improving the overall efficiency and resistance to coke formation.

3.2. Cu based catalysts

Cu as an active metal can suppress carbon formation in the syngas production step and can improve water gas shift reaction. The SMR over $5Cu/Co_6Al_2$ solid shows a high methane conversion of 96% at a temperature of 650 °C with a steam to methane ratio of 3.1.[79]

The introduction of Cu into a Ni-based catalyst has also been found to improve the water-gas shift (WGS) activity which may be because of the bimetallic Cu–Ni species

amount.[80] This was observed for SMR when 0.01 wt% Cu was added to 0.5 wt% Ni, which increased the WGS reaction rate, although no activity was observed over the 0.5 wt% pure Cu catalyst but the addition of 0.01 wt% Ni caused an increase in methane conversion rate with temperature (methane conversion occurs over Ni and not Cu).[81]

Cu metal is known to be less active for SMR in comparison to metals like Ni, Rh, Pt and Pd.[5] However, Cu-based catalysts are the most used catalysts in methanol steam reforming[82–84] and ethanol steam reforming.[85–87] The Cu/ZnO catalyst has been found to exhibit high catalyst activity for methanol reforming and the water-gas shift reaction.[88] For example, $5\%Cu_5Zn_{10}Al$ exhibited the best catalyst performance with a methanol conversion of 98% at a temperature of 350 °C under a GHSV of 15 500 h^{-1} and an H_2O/CH_3OH ratio of 2.[88]

3.3. Molybdenum-based catalysts

Mo-based catalysts are known for their coking resistance in comparison to conventional Co and Fe Fischer–Tropsch catalysts and has been used as a Ni promoter.[89] A bimetallic Mo–Ni catalyst supported on Al_2O_3 showed a low methane conversion of 30% at a temperature of 800 °C with a high H_2/CO ratio.[90] In the case of alumina-supported Mo, the conversion is about 45–95% and the methane conversion decreases to 15–40% in the absence of the support.[91] The addition of Mo as a promoter to the Ni catalyst reduced the metal surface area but increased the number of active sites. This is due to electron transfer from the Mo species to Ni, which suggests that the Mo species may block Ni active sites, ultimately decreasing the overall number of available sites.[92] For the $NiMo_2C/Al_2O_3$ catalyst at a temperature of 800 °C and a pressure of 1 atm, the catalyst performance was observed and it exhibited a stable methane and CO_2 conversion of 89.9% and 94%, respectively, while maintaining an H_2/CO ratio of 0.99 in a 15 h methane reforming test.[93]

4. Noble metal catalysts

Several noble metals, including Rh, Ru, Pt, and Pd, have been tested as catalysts for SMR when supported on Al_2O_3–MgO. Their performance follows the order: Ru > Rh > Ir > Pt > Pd, with Ru being the most active and Pt and Pd the least active.[5] However, due to their high cost, noble metals are not commercially viable for widespread use.[5,21,94]

4.1. Ru based catalysts

The reaction mechanism on Ru-based catalysts for SMR is shown in Fig. 8. It was found that methane (through activation of the C–H bond) adsorbs and dissociates, forming CH_x intermediates, with C* and CH* being the most stable surface adsorbates. This process makes the Ru catalyst surface prone to coke formation. Additionally, calculations of the activation barriers show that C–O bond formation is kinetically slower than C–H bond activation.[95]
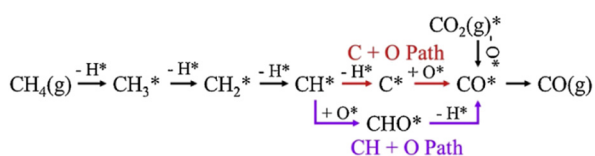
Fig. 7 Dominant reaction pathways on a cobalt catalyst.[7]

1968 | *React. Chem. Eng.*, 2025, **10**, 1963–1977

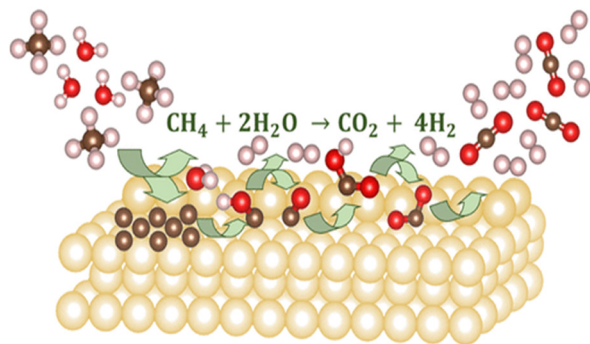This journal is © The Royal Society of Chemistry 2025

Fig. 8 Mechanism of methane reforming on a Ru catalyst.[95]

Ru has been found to be one of the most active noble metals for SMR,[96] with its ability to suppress coke formation.[97] The activities of 5 wt% Ru-based catalysts supported on alumina, ceria and ceria/alumina in the temperature range 400–800 °C are reported in Fig. 9a, where it is apparent that Ru/5Ce$_{10}$Al exhibits a higher activity than the other catalysts, Fig. 9b. Ru/Al$_2$O$_3$ exhibited the highest methane conversion with no carbon deposited on Ru/Al$_2$O$_3$ and Ru/5Ce$_{10}$Al.[97]

The addition of Ru to Ni-catalysts supported on MgO, La$_2$O$_3$, and Al$_2$O$_3$ was found to enhance the catalytic performance in the reforming reaction by improving the catalytic activity and stability and prevented coke formation.[98,99]

Ru catalysts supported on MgO, Nb$_2$O$_5\cdot n$H$_2$O and Nb$_2$O$_5$ for SMR showed high activity at a temperature of 700 °C and S/C ratio of 4 with complete methane conversion.
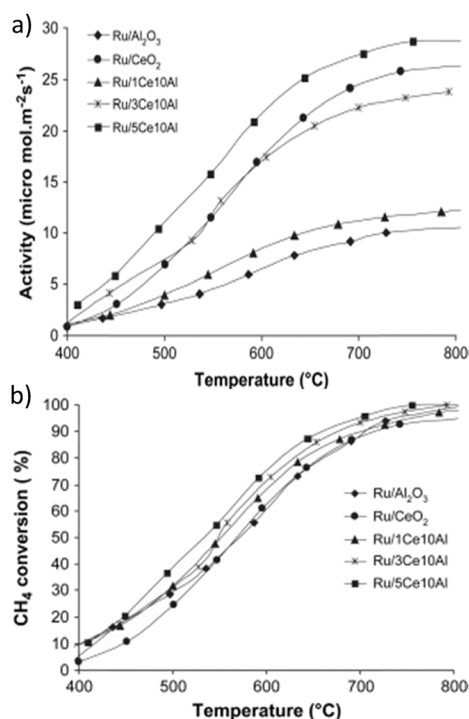

Fig. 9 a) Activity per mmol m^{-2} s^{-1} of a Ru-based catalyst between 400–800 °C. b) Methane conversion (%) of a Ru-based catalyst between 400–800 °C.[97]

However, the addition of magnesium to alumina-supported ruthenium enhanced catalyst activity by increasing the dispersion of ruthenium and decreasing the methane conversion but also prevented coke formation.[100] In the case of partial oxidation of methane over 1.0 wt% Ru/SiO$_2$ catalysts, 93.9% methane conversion was achieved with 91.6% H$_2$ and 94.6% CO selectivity.[101]

4.2. Rhodium based catalysts

Rhodium, as a transition metal, is one of the most active metals for SMR,[102] but its high cost limits its use.[103] Fig. 10 illustrates the reaction mechanism for rhodium in methane decomposition. In this process, CH$_x$ species migrate and form ethane, which is then adsorbed on the rhodium catalyst surface and dissociated to produce H$_2$. Notably, methane is adsorbed on the surface, with no other products detected on the rhodium surface.[104]

Rhodium (Rh) was found to be active in methane decomposition to produce H$_2$ when TiO$_2$ and V$_2$O$_5$ were used as promoters for Rh/Al$_2$O$_3$ in methane reforming at 773 K. Both V$_2$O$_5$ and TiO$_2$ promoted Rh/Al$_2$O$_3$ catalysts showed increased conversion, with Rh/Al$_2$O$_3$ exhibiting the best performance. This catalyst produced the highest amount of H$_2$, achieving a methane conversion of about 85% in the first pulse, compared to 46% for the V$_2$O$_5$–Al$_2$O$_3$ catalyst and 5% for pure Rh.[105] For SMR, a 0.8% Rh/Ce$_{0.6}$Zr$_{0.4}$O$_2$ catalyst achieved a methane conversion of 82% at a low temperature of 550 °C and an S/C ratio of 4.[106] Experimental tests demonstrated that methane conversion improved from 23% to 68% under similar conditions. When comparing Rh–perovskite catalysts with Ni-based catalysts, the Rh–perovskite catalyst exhibited lower carbon deposition and higher methane conversion, improving from 23% to 68%.[107]

4.3. Pt-based catalysts

Although Rh catalysts exhibit excellent catalyst performance for SMR, Pt has good catalytic performance for H$_2$ production because of its high availability and low cost compared to
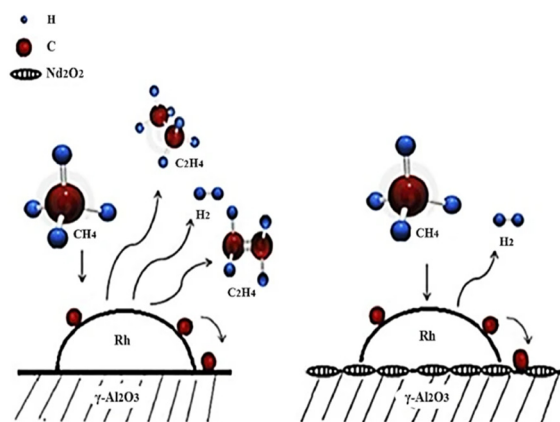

Fig. 10 Mechanism of methane decomposition over a rhodium catalyst.[104]

This journal is © The Royal Society of Chemistry 2025

React. Chem. Eng., 2025, **10**, 1963–1977 | **1969**

rhodium.[108] The addition of a Ce promoter to Pt/ZrO_2 catalysts improved the catalyst activity, stability and the H_2/CO ratio of the product syngas. High temperatures reduce the catalyst activity, however calcination and reduction at 500 °C caused a strong Pt–Ce surface interaction that formed Ce^{3+} sites which improved the dispersion of Pt.[109] In comparing a Pt $(0.5\%)/Al_2O_3$ catalyst, Pt $(0.5\%)/Al_2O_3$ catalyst and Pt (0.5%) Ni $(10\%)/Al_2O_3$ bimetallic catalyst, the bimetallic catalyst (Pt (0.5%) Ni $(10\%)/Al_2O_3$) showed the best catalyst performance during a reaction time of ~108 h at 750 °C exhibiting methane conversion from 78% to 95%, which proves that the introduction of Pt to a Ni catalyst increases the catalyst performance and limits coke formation.[109,110]

5. Steam reforming process intensification

5.1. Sorption-enhanced SMR

To address the challenges associated with SMR (increased energy consumption, coke formation on the catalyst at high temperatures, and the high cost of H_2 separation), researchers suggest sorbent-enhanced steam reforming to improve H_2 production.[111]

Sorption-enhanced SMR uses a sorbent to absorb CO_2 as it is produced. This has the advantage of enhancing the rate of the WGS reaction, improving the H_2 production rate, and producing a pure H_2 stream without the need for a separate carbon capture unit, lowering process costs.[111–113] Some of the sorbents used in SE-SMR are listed in Table 1.

The CO_2 sorption reaction in the SESMR process includes the reforming reaction in eqn (1), water–gas shift in eqn (2) and lastly the sorption reaction in eqn (4), which takes place at the same time in one reactor.[114]

$$CO_{2(g)} + \varepsilon_{(s)} \rightleftarrows CO_2\varepsilon_{(s)} \qquad (4)$$
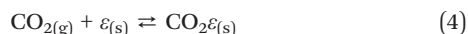
In the equation above, $\varepsilon_{(s)}$ is the sorbent for CO_2 which reacts with the carbon to form a carbonated solid. Eqn (5) shows the overall SE-SMR reaction which becomes:[115]

$$CH_{4(g)} + 2H_2O_{(g)} + \varepsilon_{(s)} \rightleftarrows CO_2\varepsilon_{(s)} + 4H_{2(g)}. \qquad (5)$$

CaO is an appealing sorbent due to its low cost and high adsorption capacity. It can be produced from natural minerals like limestone and dolomite which are readily available from a variety of sources.[116]

Comparing a conventional SMR to SESMR using an 18 wt% Ni/Al_2O_3 catalyst, the SESMR exhibited a methane conversion of 65% and H_2 purity of 85% at a temperature of 650 °C, pressure of 30 bar, and S/C ratio of 3, while the conventional SMR exhibited a methane conversion of 24% and H_2 purity of 49%.[117] A $NiO–CaO–Ca_{12}Al_{14}O_{33}$ catalyst with 25 wt% NiO showed a methane conversion of 99.1% and H_2 production efficiency of 96.1% during 10 cycles of SESMR.[118] The addition of NiO in $Ca_{12}Al_{14}O_{33}$ showed a conversion of over 80% at 650 °C with a methane-to-steam ratio of 3.4 and H_2 selectivity of 90%.[119] A $CaO–Ca_9Al_6O_{18}$ sorbent and Ni/MgAl catalyst for the SESMR process showed that a high S/C ratio, low temperature, and low space velocity improved H_2 purity, although the sorbent to catalyst ratio had no effect on the H_2 purity above 90 vol%.[120]

Farooqi et al.[121] compared the performance of $Ni/Ca_{12}Al_{14}O_{33}$, $Ni–Co/Ca_{12}Al_{14}O_{33}$, $Ni–Cu/Ca_{12}Al_{14}O_{33}$, and $Ni–Fe/Ca_{12}Al_{14}O_{33}$ catalysts in an FBR, at 700 °C, using an S/C ratio of 3. Of these, $Ni–Co/Ca_{12}Al_{14}O_{33}$ performed the best, producing the highest average H_2 purity over 10 cycles (78%) which the authors attributed to the synergistic properties of Ni and Co. In the case of carbon deactivation of Ca-based sorbents, as shown in Fig. 11, the exposure of carbon and other gas mixtures to the outer layer of CaO causes a reaction between the two that forms $CaCO_3$. The CO_2 shell migrates through pores to the inner surface of CaO which is known as the shirking core.[122] This causes the blockage of the Ca-based sorbents with reaction time, damaging the sorbent's pore structure.

Lithium zirconate (LZC) as a CO_2 sorbent has been found to offer high capacity but slow kinetics due to the enthalpy associated with the chemical bond of CO_2 on the LZC surface, although hydrotalcite (HTC) and a K-promoted HTC sorbent are the opposite showing a fast kinetics but low capacity.[123]

A Ni/MgO catalyst and K-promoted HTC sorbent were used to analyse the performance of the SESMR process (at 500 °C, 4.47 bar and S/C ratio of 6), exhibiting a H_2 purity of 96% on a dry basis and a methane conversion of 84% which are achieved at high sorbent capacity of ≥ 2 mol kg^{-1}.[123] Comparing CaO, lithium zirconate and hydrotalcite sorbent, lithium zirconate and hydrotalcite showed better sorption at 500 °C, 5 bar and S/C ratio of 3 achieving methane conversion of 91.3% and 55.2% and H_2 purity of 94.1% and 77.8% which later increased.[124]

In summary, SESMR challenges include the need for high-performance sorbents, limitations in sorbent regeneration, difficulty in maintaining long-term stability, and the complexity of integrating sorbent cycling with the reforming process.

Liu et al.[125] investigated a combining sorbent and chemical looping (section 6.5) enhanced SMR, to address the low CO_2 capture rates of sorbents at mild temperatures (500–600 °C) and low CO_2 concentrations (5–10%). In a fixed bed reactor operated at 600 °C with a S/C ratio of 4, utilising a Ni-based oxygen carrier and Li-based adsorbent achieved a methane conversion rate of 93.3%, a H_2 purity of 92.8%, and a CO_2 capture rate of 90.1%.

Table 1 Various sorbents for sorbent enhanced SMR

Natural sorbents	Synthetic sorbents
Calcium carbonate ($CaCO_3$)	Lithium orthosilicate (Li_4SiO_4)
Dolomite ($CaCO_3 \times MgCO_3$)	Lithium zirconate (Li_2ZrO_3)
Huntite ($CaCO_3 \times 3MgCO_3$)	Sodium zirconate (Na_2ZrO_3)

1970 | React. Chem. Eng., 2025, 10, 1963–1977
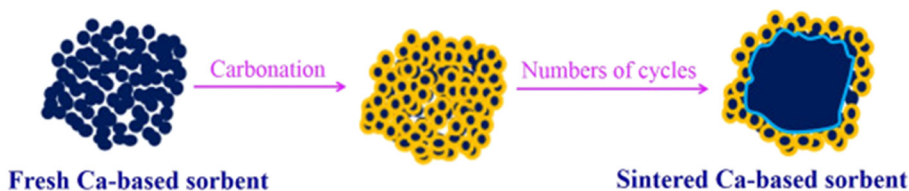
This journal is © The Royal Society of Chemistry 2025

Fig. 11 Ca-based sorbent deactivation mechanism.[122]

Furthermore, Li_4SiO_4 demonstrated sustained performance, maintaining a high CO_2 adsorption rate of 63.7% and a crushing strength exceeding 25 N even after 200 cycles.

5.2. Oxidative SMR

Oxidative SMR is an advanced technology used for an energy-efficient H_2 production process. Eqn (6) and (7) show the oxidative SMR reaction when oxygen is added to methane and steam, or methane combustion occurs.

$$CH_4 + H_2O \leftrightarrows CO + 3H_2 \qquad \Delta H = +205.8 \text{ kJ mol}^{-1} \qquad (6)$$

$$CH_4 + 2O_2 \leftrightarrows CO_2 + 2H_2O \qquad \Delta H = -803 \text{ kJ mol}^{-1} \qquad (7)$$

Ni catalysts are mostly used in conventional steam reforming but the addition of oxygen to the reaction can cause Ni to oxidise and lose its activity. Hence, the addition of small amounts of noble metals can be used to increase Ni's stability during oxidative SMR.[126] The addition of noble metals such as Rh, Pt and Pd to NiO–MgO and Ni/γ-Al_2O_3 helps to reduce coke deposition, but hot-spot formation SMR can result in the formation of noble metal atoms segregated on the metal particle surface.[127] Furthermore, this technique requires the need for a precise balance between oxygen and methane to avoid side reactions and ensure stable performance.

5.3. Plasma and electrical field enhanced SMR

Plasma SMR is similar to the conventional SMR, but plasma provides radicals and energetic species generated from electricity.[128] Cold plasma and warm plasma are examples of non-thermal plasmas that can be used to produce hydrogen on a small scale, although warm plasmas are better in terms of hydrogen efficiency and rate.[129]

Choi et al.[130] compared catalytic SMR, plasma SMR, and a combination of both techniques. A microwave, set to 6 kW, was used to produce plasma, and a NiO catalyst was used for catalytic and combined SMR. A S/C ratio of 3.7 was used throughout. Plasma and catalytic SMR produced syngas with a H_2 concentration of 67%, while combined SMR's product contained 75% H_2. Combined SMR also demonstrated the highest methane conversion (92%) as compared to plasma SMR's conversion of 69% and catalytic SMR's conversion of 64%. However, catalytic SMR produced the highest energy efficiency of 55%, compared to plasma and combined SMR's efficiencies of 43% and 46%, hence the methane conversion

between catalytic and combined SMR is similar from an energy perspective. It was also noted by the authors that increasing the S/C ratio to 4.7 caused the methane conversion, energy efficiency, and H_2 purity of plasma SMR to increase to 60%, 95%, and 77%, respectively. Hence the authors concluded that optimised steam plasma reforming has high potential to enhance SMR. In a comparative study by Garcia-Villalva et al.,[131] plasma SMR demonstrated better performance than plasma methane reforming (MR) and plasma dry methane reforming (DMR). Plasma SMR achieved a methane conversion of 24% and an H_2 yield of 80%, whereas plasma MR and plasma DMR attained methane conversion rates of 12% and 19%, and H_2 yields of 73% and 48%, respectively. This study also identified Ni/Al_2O_3 and Ni/CeO_2 as promising catalysts for catalytically enhanced plasma SMR, a future research route.[132] Electrical field enhanced SMR uses an electric current to enhance the activity of SMR catalysts.[133] Electrical field enhanced SMR over Ni–CeO_2/γ-Al_2O_3–MgO achieved a methane conversion of 96.4% and H_2 yield of 75.3% at 600 °C.[132] At 262 °C, a Pt catalyst supported on $Ce_xZr_{1-x}O_2$ solid solution exhibited a methane conversion of 40.6%.[134] This technique is still limited by high energy consumption, limited catalyst compatibility, difficulty in achieving uniform temperature control, and challenges in scaling up the process for industrial applications.

In a study by Lu et al.,[135] the scalability of an electric field-enhanced SMR was analysed. This investigation focused on a fixed bed reactor with a height of 0.88 m and a diameter of 0.5 m. Notably, it was found that the reactor's cross-sectional temperature profile remained largely uniform, representing a significant advantage over conventional SMR when scaled.

5.4. Photocatalytic and thermo-photo hybrid SMR

Photocatalytic SMR involves the use of semiconductors and sunlight; the semiconductors cause the breaking of the C–H bond of methane and the ability for water splitting by photocatalytic oxidative activity.[136] TiO_2 is mostly used as a photocatalyst in photocatalytic SMR.[137] $SrTiO_3$ photocatalysts, although show moderate activity and are not expensive, have low adsorption of methane, hence there is a need for cocatalysts like noble metals Rh, Pt, and Ru in PSMR.[136] A high rate of hydrogen was produced when Pt/$CaTiO_3$ photocatalysts were used in PSMR.[138] Rh in $K_2Ti_6O_{13}$ increased the speed of the photocatalytic reaction with Rh

oxide and Rh metal acting as promoters to oxidize and reduce the reaction, respectively, as shown in Fig. 12.[138]

Silver is known to improve the $SrTiO_3$ photocatalytic activity in photocatalysis and thermocatalysis processes by dissociating methane to form Ag–H bonds. Ag^+ was regarded as the oxidation reaction site while adsorbing the methane molecules and Ag^0 acted as the reduction reaction site in the process while consuming low energy.[136]

The thermo-photo hybrid process was demonstrated with a Pt/black TiO_2 catalyst by filtering UV light from AM 1.5G sunlight, causing methane and steam to produce syngas without a water-gas shift.[139] The result of this was an increased H_2 yield of 185 mmol h^{-1} g^{-1} with a quantum efficiency of 60% achieved at 500 °C.[139] Photocatalytic and thermo-photo hybrid SMR face challenges such as low efficiency under practical conditions, limited catalyst stability and scalability, and difficulties in optimizing the balance between light absorption and heat management for sustained methane conversion.

5.5. Chemical looping SMR

Chemical SMR utilises an oxygen carrier, that often doubles as a catalyst, to oxidise methane, enhancing the production of H_2.[133] The metal oxide is then regenerated in an air reactor as shown in Fig. 13, where the metal oxide oxygen carrier is represented as MeO_x. MeO_x is reduced by methane to produce $MeO_{x-\delta 1-\delta 2}$ and syngas, $MeO_{x-\delta 1-\delta 2}$ is then oxidised by steam to recover most of the lattice oxygen to $MeO_{x-\delta 1}$ (the intermediate state) which produces hydrogen and finally, the intermediate state is oxidized through air oxidation to MeO_x (the original state).[140] The advantage of this technology is that the oxygen carrier/catalyst can be continuously regenerated, reducing tar and coke production, and that heat released from oxidation of MeO_x can be used to maintain the temperature of the reforming reactor, potentially making the process autothermal.[141,142]

Yang et al.[143] investigated the use of a Ni loaded Fe_2O_3/Al_2O_3 oxygen carrier for methane reforming. Using a 10% $NiO–Fe_2O_3/Al_2O_3$ catalyst at 950 °C, a methane conversion of 96% and H_2 yield of 3.3 mmol g^{-1} were obtained. Under these conditions, a low carbon build up (0.093 mmol g^{-1}) was observed, indicating the stability of this oxygen carrier. Hu et al.[144] proposed the use of Ni/Fe modified calcite as a sustainable oxygen carrier. Calcite is
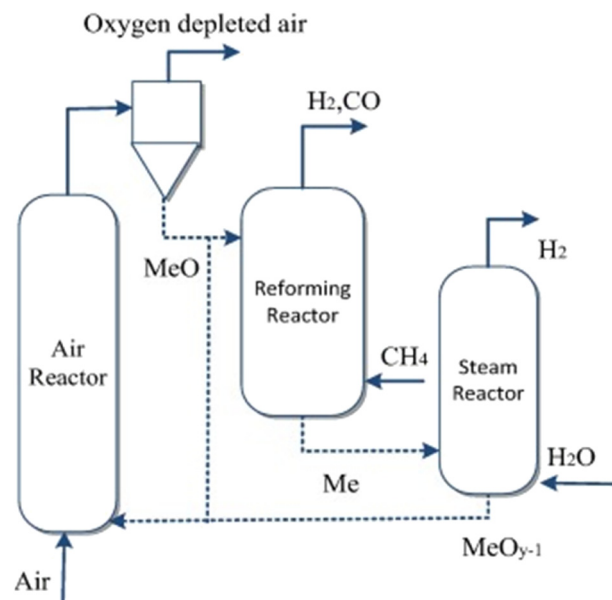

Fig. 13 Chemical looping SMR process for hydrogen production.[140]

a natural mineral and so it's use would reduce the cost of producing the oxygen carrier. Using a temperature of 800 °C, a steam/oxygen carrier ratio of 0.67, and a methane/oxygen carrier ratio of 0.13, the average methane conversion, H_2 yield, and carbon deposition produced over a 180 min period were 96.01%, 7.04 mol kg^{-1}, and 3.28% respectively. This indicates the promise that modified natural ore oxygen carriers have for SMR.

$La_{1-x}MnCu_xO_3$ and Fe, Co and Ni in $LaMnO_{3+\delta}$ have been found to show excellent activity and stability while reducing coke formation during multiple cycles, exhibiting good oxygen ion mobility.[145,146] Yin et al.[147] investigated the use of $LaMnO_{3+\delta}$, $LaMn_{0.7}Fe_{0.3}O_{3+\delta}$, $LaMn_{0.8}Co_{0.2}O_{3+\delta}$ and $LaMn_{0.9}Ni_{0.1}O_{3+\delta}$ as oxygen carriers. From this, it was found that $LaMn_{0.7}Fe_{0.3}O_{3+\delta}$ and $LaMn_{0.8}Co_{0.2}O_{3+\delta}$ oxygen carriers performed the best, producing a H_2 yield of 0.6 mmol g^{-1} and 0.8 mmol g^{-1}, respectively after twenty 10 minute cyclic tests at 850 °C.

Current chemical looping SMR challenges include the need for complex reactor designs, limited oxygen carrier stability, the potential for high material costs, and challenges in maintaining efficient cyclic operation at high temperatures.

5.6. Membrane reactors for SMR

Membrane reactors for SMR allow the removal of hydrogen by a shift in equilibrium according to Le Chatelier's principle, which improves the methane conversion and product yield of the reaction at mild temperatures.[148–150]

Palladium (Pd) membranes have an incredibly high H_2 separation efficiency (>99.9999%) and excellent mechanical properties. However, their high cost and chemical instability have prevented their large-scale application.[151] It has been
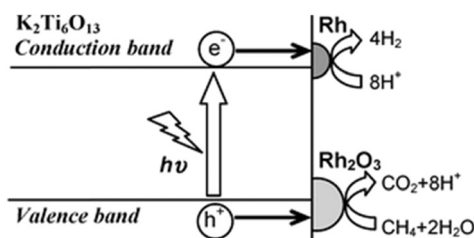

Fig. 12 Rh/Rh_2O_3/$K_2Ti_6O_{13}$ photocatalyst's reaction mechanism for PSMR.[138]

1972 | React. Chem. Eng., 2025, 10, 1963–1977

This journal is © The Royal Society of Chemistry 2025

noted that Pd–Ag alloys have an even higher H_2 selectivity than pure Pd membranes, hence Nemitallah et al.[152] produced a model to simulate the performance of a Pd–Ag membrane reactor for SMR. This model suggests that a co-current flow configuration, high feed pressure, inlet gas temperature, and H_2 concentrations result in H_2 flux across the membrane. The recent literature has explored the use of Ni-based membranes due to their lower cost and higher stability. Wang et al.[153] investigated a Ni hollow fibre membrane and found that at 1000 °C and a S/methane ratio of 3, the H_2 production rate reached 50.84 mmol m^{-2} s^{-1}, and it possessed high resistance to coke formation at temperatures exceeding 800 °C. Although membrane reactors for SMR are promising, they face limitations including susceptibility to coke formation, membrane degradation at high temperature and pressure, reduced hydrogen selectivity, high material costs, and challenges in long-term stability and integration with existing systems that need to be addressed to enable their widespread use.

5.7. Methane fuelled solid oxide fuel cells

Solid oxide fuel cells (SOFCs) directly convert stored chemical energy in fuels (natural gas, carbon monoxide or biogas) into electricity and H_2.[154] They have been found to offer commercial applications because of their increased energy efficiency and their fuel flexibility.[155] Solid oxide fuel cell devices have high conversion efficiency, provide low pollution emission and zero noise. Among the fuels used by SOFCs, methane may be the best fuel due to its abundance in natural gas and easy conversion from CO_2 and/or biomass with the use of efficient catalysts to improve the methane conversion rate.[156]

Using 10%CH_4–5%O_2–5%CO_2 as fuel, a maximum power density of 1321.5 mW cm^2 was achieved at 800 °C. The addition of 5%CO_2 caused an increase in methane conversion (from 31.69% to 50.03%) and coke tolerance.[157] Although the interaction between Ni and yttria-stabilised zirconia (YSZ) is weak, the interaction of samarium to the Ni–YSZ (yttria-stabilised zirconia) anode cell formed smaller particles and excellent interfacial contact, which achieved a maximum power density of 1.54 W cm^{-2} for methane fuel at 800 °C.[158] The addition of La to the Ni–YSZ anode results in increased activity for methane reforming and electrochemical oxidation of hydrogen.[158] An n = 2 Ruddlesden–Popper (RP) phases $La_{1.5}Sr_{1.5}Mn_{1.5}Ni_{0.5}O_{7\pm\delta}$ with 82 mol% methane, 18 mol% N_2 and a low S/C of 0.15 showed a methane conversion of 14.60 mol% and H_2 production of 24.19 mol% for more than 4 h.[159]

In a recent study conducted by Zhang et al.,[160] a MgO-modified Ni_3Sn anode was investigated for applications within methane-fuelled SOFCs. The synergistic effects of MgO and Sn were found to enhance charge transfer and full gas diffusion within the anode. This modification also reduced coke buildup by promoting the preferential oxidation of carbon atoms, preventing coke accumulation.

This cell demonstrated a power density of 374 mW cm^{-2} and exhibited great stability over an operation period of 100 hours at 700 °C using humidified methane as a fuel.

SOFCs for SMR face challenges that can be summarized as high operating temperatures, susceptibility to carbon deposition (coking) and the need for complex fuel reforming systems to efficiently convert methane.

6. Conclusion and outlook

SMR state-of-the-art and novel technologies have been reviewed, focusing on the key issues of SMR catalysts and recent development of new promoters such as noble metals (Ru, Rh, Pt, Ir, Ag, and Au), alkali metals (e.g., K), rare earth metals (e.g., Ce and Nb), metal oxides (MgO, CaO, and La_2O_3) and non-metal like boron. Solid solution catalysts were discussed and found to enhance Ni catalyst activity when a 20 wt% NiO/MgO solid-solution catalyst exhibited a methane conversion of 91% at an S/C ratio of 1/1 at atmospheric pressure and a temperature 800 °C. Structural improvement of SMR catalysts was also highlighted in the literature review to help improve the catalyst activity and stability by Ni particle size control, surface morphology of the catalyst, metal oxide substrates and self-supporting catalysts. The review gave a comprehensive analysis of non-noble metal catalysts (Co, Cu, and Mo) and noble metal catalysts (Ru, Rh, and Pt). Moreover, a discussion of the advanced SMR process has been proposed, to improve the H_2 productivity and reduce the energy demand. The most promising advanced SMR techniques include membrane reactors, which offer efficient hydrogen separation and higher selectivity, and chemical looping, which enables CO_2 capture and improves methane conversion while reducing energy consumption. Additionally, photocatalytic and plasma-enhanced reforming methods show potential for lower energy input and cleaner processes, although challenges remain in scaling and optimizing these technologies for industrial use.

From this review current research trends tend towards the use of supported bimetallic catalysts, with Ni–Co/Al_2O_3 consistently demonstrating high activity and good stability. Further research must be conducted to enhance the performance of these catalysts, optimise process conditions, and support structure, and life cycle analyses to assess the sustainability of these catalysts. Advanced SMR technologies such as membrane reactors, sorption enhancement, and chemical looping have demonstrated their value in improving methane conversion and H_2 purity. Techno economic analyses of these technologies must be conducted to assess their commercial viability, and potential combinations (such as sorption enhanced SMR conducted in a membrane reactor) should be explored. Recent studies have also been exploring the application of SMR technologies to other feedstocks, such as glycerol, ethanol, and methanol, improving the feed flexibility of the technology and improving its viability industrially.

Data availability

No primary research results, software or code have been included and no new data were generated or analysed as part of this review.

Conflicts of interest

There are no conflicts to declare.

References

1 I. E. Agency, *Global Energy Review 2025*, Paris, 2025.

2 C. Le Quéré, G. P. Peters, P. Friedlingstein, R. M. Andrew, J. G. Canadell, S. J. Davis, R. B. Jackson and M. W. Jones, *Nat. Clim. Change*, 2021, **11**, 197–199.

3 K. Mazloomi and C. Gomes, *Renewable Sustainable Energy Rev.*, 2012, **16**, 3024–3033.

4 H. L. Yip, A. Srna, A. C. Y. Yuen, S. Kook, R. A. Taylor, G. H. Yeoh, P. R. Medwell and Q. N. Chan, *Appl. Sci.*, 2019, **9**, 4842.

5 H. Zhang, Z. Sun and Y. H. Hu, *Renewable Sustainable Energy Rev.*, 2021, **149**, 111330.

6 I. E. Agency, *Global Hydrogen Review 2023*, Paris, 2023.

7 L. Chen, Z. Qi, S. Zhang, J. Su and G. A. Somorjai, *Catalysts*, 2020, **10**, 858.

8 C. Park, S. Oh, C. Kim, Y. Choi and Y. Ha, *Fuel*, 2021, **287**, 119501.

9 I. Karpilov, V. Papkov and D. Pashchenko, *Int. Commun. Heat Mass Transfer*, 2024, **159**, 108322.

10 S. Nogales-Delgado, C. M. Álvez-Medina, V. Montes and J. F. González, *Catalysts*, 2023, **13**, 1482.

11 W. Nabgan, T. A. T. Abdullah, R. Mat, B. Nabgan, Y. Gambo, M. Ibrahim, A. Ahmad, A. A. Jalil, S. Triwahyono and I. Saeh, *Renewable Sustainable Energy Rev.*, 2017, **79**, 347–357.

12 M. G. Martínez, M. Elsaddik and A. Nzihou, *Int. J. Hydrogen Energy*, 2023, **48**, 22113–22131.

13 M. Taji, M. Farsi and P. Keshavarz, *Int. J. Hydrogen Energy*, 2018, **43**, 13110–13121.

14 E. Baraj, K. Ciahotný and T. Hlinčík, *Fuel*, 2021, **288**, 119817.

15 S. M. Soltani, A. Lahiri, H. Bahzad, P. Clough, M. Gorbounov and Y. Yan, *Carbon Capture Sci. Technol.*, 2021, **1**, 100003.

16 J. R. Rostrup-Nielsen, *Catal. Today*, 2023, **423**, 113878.

17 A. Pafili, N. D. Charisiou, S. L. Douvartzides, G. I. Siakavelas, W. Wang, G. Liu, V. G. Papadakis and M. A. Goula, *Catalysts*, 2021, **11**, 1526.

18 A. Ochoa, J. Bilbao, A. G. Gayubo and P. Castaño, *Renewable Sustainable Energy Rev.*, 2020, **119**, 109600.

19 J. M. Ginsburg, J. Piña, T. El Solh and H. I. De Lasa, *Ind. Eng. Chem. Res.*, 2005, **44**, 4846–4854.

20 M. D. Argyle and C. H. Bartholomew, *Catalysts*, 2015, **5**, 145–269.

21 E. Meloni, M. Martino and V. Palma, *Catalysts*, 2020, **10**, 352.

22 C. V. Satyanarayana, D. Srikant and H. R. Gurav, in *Industrial Catalytic Processes for Fine and Specialty Chemicals*, ed. S. S. Joshi and V. V. Ranade, Elsevier, Amsterdam, 2016, pp. 187–219, DOI: **10.1016/B978-0-12-801457-8.00005-7**.

23 P. Forzatti and L. Lietti, *Catal. Today*, 1999, **52**, 165–181.

24 F. Boshagh, H.-J. Yoon and C.-J. Lee, *Renewable Sustainable Energy Rev.*, 2025, **218**, 115777.

25 F. Zarei-Jelyani, F. Salahi, M. Farsi and M. Reza Rahimpour, *Fuel*, 2022, **324**, 124785.

26 F. Morales-Cano, L. F. Lundegaard, R. R. Tiruvalam, H. Falsig and M. S. Skjøth-Rasmussen, *Appl. Catal., A*, 2015, **498**, 117–125.

27 M. S. Ferrandon, C. Byron, G. Celik, Y. Zhang, C. Ni, J. Sloppy, R. A. McCormick, K. Booksh, A. V. Teplyakov and M. Delferro, *Appl. Catal., A*, 2022, **629**, 118379.

28 C. H. Bartholomew, *Appl. Catal., A*, 2001, **212**, 17–60.

29 S. Sengodan, R. Lan, J. Humphreys, D. Du, W. Xu, H. Wang and S. Tao, *Renewable Sustainable Energy Rev.*, 2018, **82**, 761–780.

30 Y.-H. C. Chin, D. L. King, H.-S. Roh, Y. Wang and S. M. Heald, *J. Catal.*, 2006, **244**, 153–162.

31 Y. Xu, C. Fan, Y.-A. Zhu, P. Li, X.-G. Zhou, D. Chen and W.-K. Yuan, *Catal. Today*, 2012, **186**, 54–62.

32 V. Chihaia, K. Sohlberg, M. Dan, M. Mihet, A. R. Biris, P. Marginean, V. Almasan, G. Borodi, F. Watanabe and A. S. Biris, *React. Kinet., Mech. Catal.*, 2012, **105**, 173–193.

33 Y. Khani, N. Safari, F. Bahadoran, S. Soltanali and A. Zamaniyan, *Ind. Eng. Chem. Res.*, 2021, **60**, 9669–9683.

34 P. Tarifa, C. Megías-Sayago, F. Cazaña, M. González-Martín, N. Latorre, E. Romeo, J. J. Delgado and A. Monzón, *Energy Fuels*, 2021, **35**, 17212–17224.

35 X. Yang, J. Da, H. Yu and H. Wang, *Fuel*, 2016, **179**, 353–361.

36 N. A. Abd Ghani, A. Azapour, A. F. A. S. Muhammad and B. Abdullah, *Int. J. Hydrogen Energy*, 2019, **44**, 20881–20888.

37 Z. He, Y. Jiao, J. Wang and Y. Chen, *J. Anal. Appl. Pyrolysis*, 2016, **122**, 142–150.

38 M. Dan, M. Mihet and M. D. Lazar, *Int. J. Hydrogen Energy*, 2020, **45**, 26254–26264.

39 H.-M. Kim, W.-J. Jang, S.-Y. Yoo, J.-O. Shim, K.-W. Jeon, H.-S. Na, Y.-L. Lee, B.-H. Jeon, J. W. Bae and H.-S. Roh, *Int. J. Hydrogen Energy*, 2018, **43**, 262–270.

40 A. H. Fakeeha, A. A. Bagabas, M. S. Lanre, A. I. Osman, S. O. Kasim, A. A. Ibrahim, R. Arasheed, A. Alkhalifa, A. Y. Elnour and A. E. Abasaeed, *Processes*, 2020, **8**, 522.

41 D.-W. Jeong, W.-J. Jang, J.-O. Shim, H.-S. Roh, I. H. Son and S. J. Lee, *Int. J. Hydrogen Energy*, 2013, **38**, 13649–13654.

42 J. Xu and M. Saeys, *J. Catal.*, 2006, **242**, 217–226.

43 J. Xu, L. Chen, K. F. Tan, A. Borgna and M. Saeys, *J. Catal.*, 2009, **261**, 158–165.

44 M.-M. Millet, A. V. Tarasov, F. Girgsdies, G. Algara-Siller, R. Schlögl and E. Frei, *ACS Catal.*, 2019, **9**, 8534–8546.

45 V. Danghyan, A. Kumar, A. Mukasyan and E. Wolf, *Appl. Catal., B*, 2020, **273**, 119056.

46 Y. Wang, H. Wang, A. H. Dam, L. Xiao, Y. Qi, J. Niu, J. Yang, Y.-A. Zhu, A. Holmen and D. Chen, *Catal. Today*, 2020, **355**, 139–147.

47 D. Ligthart, R. Van Santen and E. Hensen, *J. Catal.*, 2011, **280**, 206–220.

48 L. Råberg, M. Jensen, U. Olsbye, C. Daniel, S. Haag, C. Mirodatos and A. O. Sjåstad, *J. Catal.*, 2007, **249**, 250–260.

49 D. Pashchenko, *Fuel*, 2023, **353**, 129205.

50 H. Tamagawa, K. Oyama, T. Yamaguchi, H. Tanaka, H. Tsuiki and A. Ueno, *J. Chem. Soc., Faraday Trans. 1*, 1987, **83**, 3189–3197.

51 B. Bej, N. C. Pradhan and S. Neogi, *Catal. Today*, 2013, **207**, 28–35.

52 L. He, Y. Ren, B. Yue, S. C. E. Tsang and H. He, *Processes*, 2021, **9**, 706.

53 M.-S. Jang, E. H. Cho, K. Y. Koo, W. L. Yoon and C. H. Ko, *Appl. Catal., A*, 2017, **530**, 211–216.

54 E. H. Cho, K. Y. Koo, H. W. Lee, Y.-K. Park, W. L. Yoon and C. H. Ko, *Int. J. Hydrogen Energy*, 2017, **42**, 18350–18357.

55 X. Wen, R. Li, Y. Yang, J. Chen and F. Zhang, *Appl. Catal., A*, 2013, **468**, 204–215.

56 E. Cho, Y. J. Yu, Y. Kim, T. N. Phan, D. Park and C. H. Ko, *Catal. Today*, 2020, **352**, 157–165.

57 Y. Lu, D. Guo, Y. Ruan, Y. Zhao, S. Wang and X. Ma, *J. CO2 Util.*, 2018, **24**, 190–199.

58 A. Abdulrasheed, A. Jalil, M. Hamid, T. Siang, N. Fatah, S. Izan and N. Hassan, *Int. J. Hydrogen Energy*, 2020, **45**, 18549–18561.

59 C. Wu, V. Dupont, M. A. Nahil, B. Dou, H. Chen and P. T. Williams, *J. Energy Inst.*, 2017, **90**, 276–284.

60 Q. Zhang, X. Feng, J. Liu, L. Zhao, X. Song, P. Zhang and L. Gao, *Int. J. Hydrogen Energy*, 2018, **43**, 11056–11068.

61 S. K. Chawl, M. George, F. Patel and S. Patel, *Procedia Eng.*, 2013, **51**, 461–466.

62 P. M. Araújo, K. M. da Costa and F. B. Passos, *Int. J. Hydrogen Energy*, 2021, **46**, 24107–24116.

63 J.-A. Villoria, N. Mota, S. Al-Sayari and M.-C. Álvarez-Galván, *Micro Nanosyst.*, 2012, **4**, 231–252.

64 Z. Xu, M. Zhen, Y. Bi and K. Zhen, *Catal. Lett.*, 2000, **64**, 157–161.

65 I. Iglesias, G. Baronetti and F. Mariño, *Int. J. Hydrogen Energy*, 2017, **42**, 29735–29744.

66 Y. Xu, T. Harimoto, L. Wang, T. Hirano, H. Kunieda, Y. Hara and Y. Miyata, *Chem. Eng. Process.*, 2018, **129**, 63–70.

67 T. Hirano and Y. Xu, *Int. J. Hydrogen Energy*, 2017, **42**, 30621–30629.

68 B. Li, X. Lin, Y. Luo, X. Yuan and X. Wang, *Fuel Process. Technol.*, 2018, **176**, 153–166.

69 C. Dai, S. Zhang, A. Zhang, C. Song, C. Shi and X. Guo, *J. Mater. Chem. A*, 2015, **3**, 16461–16468.

70 L. Xu, H. Zhao, H. Song and L. Chou, *Int. J. Hydrogen Energy*, 2012, **37**, 7497–7511.

71 D. Svetlizky, H. Kazimierczak, B. Ovadia, A. Sharoni and N. Eliaz, *Materials*, 2021, **14**, 834.

72 H.-W. Kim, K.-M. Kang, H.-Y. Kwak and J. H. Kim, *Chem. Eng. J.*, 2011, **168**, 775–783.

73 A. Abdulrasheed, A. Jalil, M. Hamid, T. Siang and T. Abdullah, *J. CO2 Util.*, 2020, **37**, 230–239.

74 A. I. Paksoy, B. S. Caglayan and A. E. Aksoylu, *Appl. Catal., B*, 2015, **168**, 164–174.

75 M. Schubert, S. Pokhrel, A. Thomé, V. Zielasek, T. M. Gesing, F. Roessner, L. Mädler and M. Bäumer, *Catal. Sci. Technol.*, 2016, **6**, 7449–7460.

76 E. Ruckenstein and H. Wang, *Appl. Catal., A*, 2000, **204**, 257–263.

77 D. San-José-Alonso, J. Juan-Juan, M. Illán-Gómez and M. Román-Martínez, *Appl. Catal., A*, 2009, **371**, 54–59.

78 Q. Shen, Y. Jiang, F. Xia, B. Wang, X. Lv, W. Ye and G. Yang, *Pet. Sci. Technol.*, 2020, **38**, 618–625.

79 D. Homsi, S. Aouad, C. Gennequin, J. El Nakat, A. Aboukaïs and E. Abi-Aad, *C. R. Chim.*, 2014, **17**, 454–458.

80 T.-J. Huang and S.-Y. Jhao, *Appl. Catal., A*, 2006, **302**, 325–332.

81 T.-J. Huang, T.-C. Yu and S.-Y. Jhao, *Ind. Eng. Chem. Res.*, 2006, **45**, 150–156.

82 C. Azenha, T. Lagarteira, C. Mateos-Pedrero and A. Mendes, *Int. J. Hydrogen Energy*, 2021, **46**, 17490–17499.

83 A. Lytkina, N. Zhilyaeva, M. Ermilova, N. Orekhova and A. Yaroslavtsev, *Int. J. Hydrogen Energy*, 2015, **40**, 9677–9684.

84 Y. Khani, F. Bahadoran, N. Safari, S. Soltanali and S. A. Taheri, *Int. J. Hydrogen Energy*, 2019, **44**, 11824–11837.

85 N. Homs, J. Llorca and P. R. de la Piscina, *Catal. Today*, 2006, **116**, 361–366.

86 E. Finocchio, I. Rossetti and G. Ramis, *Int. J. Hydrogen Energy*, 2013, **38**, 3213–3225.

87 D. Cao, F. Zeng, Z. Zhao, W. Cai, Y. Li, H. Yu, S. Zhang and F. Qu, *Fuel*, 2018, **219**, 406–416.

88 S. T. Yong, C. W. Ooi, S.-P. Chai and X. Wu, *Int. J. Hydrogen Energy*, 2013, **38**, 9541–9552.

89 T. Li, M. Virginie and A. Y. Khodakov, *Appl. Catal., A*, 2017, **542**, 154–162.

90 L. Dehimi, M. Gaillard, M. Virginie, A. Erto and Y. Benguerba, *Int. J. Hydrogen Energy*, 2020, **45**, 24657–24669.

91 T. Christofoletti, J. M. Assaf and E. M. Assaf, *Chem. Eng. J.*, 2005, **106**, 97–103.

92 S. Maluf and E. Assaf, *Fuel*, 2009, **88**, 1547–1553.

93 Y. Duan, R. Shang, X. Zhong, W. Xie, X. Wang and L. Huang, *Int. J. Hydrogen Energy*, 2016, **41**, 21955–21964.

94 Q. Guo, J. Geng, J. Pan, L. Zou, Y. Tian, B. Chi and J. Pu, *Energy Rev.*, 2023, 100037.

95 R. L. Arevalo, S. M. Aspera, M. C. Sison Escaño, H. Nakanishi and H. Kasai, *ACS Omega*, 2017, **2**, 1295–1301.

96 G. Jones, J. G. Jakobsen, S. S. Shim, J. Kleis, M. P. Andersson, J. Rossmeisl, F. Abild-Pedersen, T. Bligaard, S. Helveg and B. Hinnemann, *J. Catal.*, 2008, **259**, 147–160.

97 M. Safariamin, L. H. Tidahy, E. Abi-Aad, S. Siffert and A. Aboukaïs, *C. R. Chim.*, 2009, **12**, 748–753.

98 A. Ishihara, E. W. Qian, I. N. Finahari, I. P. Sutrisna and T. Kabe, *Fuel*, 2005, **84**, 1462–1468.

99 S. Andraos, R. Abbas-Ghaleb, D. Chlala, A. Vita, C. Italiano, M. Laganà, L. Pino, M. Nakhl and S. Specchia, *Int. J. Hydrogen Energy*, 2019, **44**, 25706–25716.

This journal is © The Royal Society of Chemistry 2025

React. Chem. Eng., 2025, **10**, 1963–1977 | 1975

100 L. S. Carvalho, A. R. Martins, P. Reyes, M. Oportus, A. Albonoz, V. Vicentini and M. do Carmo Rangel, *Catal. Today*, 2009, **142**, 52–60.

101 Q. Yan, T. Wu, W. Weng, H. Toghiani, R. Toghiani, H. Wan and C. Pittman Jr, *J. Catal.*, 2004, **226**, 247–259.

102 T. G. de Araújo Moreira, J. F. S. de Carvalho Filho, Y. Carvalho, J. M. A. R. de Almeida, P. N. Romano and E. F. Sousa-Aguiar, *Fuel*, 2021, **287**, 119536.

103 A. Saeedi and F. Zangooei, *Hydrogen, Fuel Cell Energy Storage*, 2024, **11**, 169–178.

104 M. Caballero, G. Del Angel, A. Bonilla-Sánchez, I. Rangel-Vázquez, A. Arrieta, A. Vázquez-Zavala, L. Huerta and M. Salgado, *Int. J. Hydrogen Energy*, 2016, **41**, 23247–23259.

105 I. Sarusi, K. Fodor, K. Baán, A. Oszkó, G. Pótári and A. Erdőhelyi, *Catal. Today*, 2011, **171**, 132–139.

106 M. H. Halabi, M. H. J. M. de Croon, J. van der Schaaf, P. D. Cobden and J. C. Schouten, *Appl. Catal., A*, 2010, **389**, 80–91.

107 R. Chava, B. A. V. D, B. Roy and S. Appari, *J. CO2 Util.*, 2022, **65**, 102206.

108 N. Ruban, V. Rogozhnikov, O. Stonkus, V. Emelyanov, V. Pakharukova, D. A. Svintsitskiy, S. Zazhigalov, A. Zagoruiko, P. Snytnikov and V. Sobyanin, *Fuel*, 2023, **352**, 128973.

109 A. L. A. Marinho, Development of catalytic process for biogas upgrading: study of structure and oxygen mobility on Ni and Pt nanoparticles encapsulated catalysts, *PhD*, Université de Poitiers; Universidade federal do Rio de Janeiro, 2020.

110 I. R. Azevedo, A. A. Da Silva, Y. T. Xing, R. C. Rabelo-Neto, N. T. Luchters, J. C. Fletcher, F. B. Noronha and L. V. Mattos, *Int. J. Hydrogen Energy*, 2022, **47**, 15624–15640.

111 Y. Wang, M. Z. Memon, M. A. Seelro, W. Fu, Y. Gao, Y. Dong and G. Ji, *Int. J. Hydrogen Energy*, 2021, **46**, 23358–23379.

112 Y. Hu, L. Liu, K. Xu, Y. Song, J. Jing, H. Zhang and J. Feng, *Carbon Resour. Convers.*, 2023, **6**, 132–141.

113 D. B. L. Santos, A. C. P. Oliveira and C. E. Hori, *J. CO2 Util.*, 2021, **51**, 101634.

114 M. M. Shahid, S. Z. Abbas, F. Maqbool, S. Ramirez-Solis, V. Dupont and T. Mahmud, *J. Environ. Chem. Eng.*, 2021, **9**, 105863.

115 A. Di Giuliano and K. Gallucci, *Chem. Eng. Process.*, 2018, **130**, 240–252.

116 Y. Luo, J. Chen and T. Wang, *ACS Omega*, 2024, **9**, 5330–5337.

117 S. Z. Abbas, V. Dupont and T. Mahmud, *Int. J. Hydrogen Energy*, 2017, **42**, 2889–2903.

118 H. R. Radfarnia and M. C. Iliuta, *Chem. Eng. Sci.*, 2014, **109**, 212–219.

119 C. S. Martavaltzi and A. A. Lemonidou, *Chem. Eng. Sci.*, 2010, **65**, 4134–4140.

120 M. Xie, Z. Zhou, Y. Qi, Z. Cheng and W. Yuan, *Chem. Eng. J.*, 2012, **207**, 142–150.

121 A. S. Farooqi, M. Z. Shahid, M. Essalhi, M. M. Hossain, M. M. Abdelnaby, M. A. Sanhoob, V. Manovic and M. A. Nemitallah, *Catal. Today*, 2025, **454**, 115281.

122 X. Ma, Y. Li, X. Huang, T. Feng and M. Mu, *Process Saf. Environ. Prot.*, 2021, **155**, 325–342.

123 M. Halabi, M. De Croon, J. Van Der Schaaf, P. Cobden and J. Schouten, *Chem. Eng. J.*, 2011, **168**, 872–882.

124 J. Fernandez, J. Abanades and R. Murillo, *Chem. Eng. Sci.*, 2012, **84**, 1–11.

125 M. Liu, Y. Liu, Y. Li, X. Wang, Y. Pan and H. Jin, *Chem. Eng. J.*, 2024, **498**, 155522.

126 K. Yoshida, K. Okumura, T. Miyao, S. Naito, S.-I. Ito, K. Kunimori and K. Tomishige, *Appl. Catal., A*, 2008, **351**, 217–225.

127 K. Tomishige, *J. Jpn. Pet. Inst.*, 2007, **50**, 287–298.

128 O. Akande and B. Lee, *Int. J. Hydrogen Energy*, 2022, **47**, 2874–2884.

129 X. Zhu, X. Liu, H.-Y. Lian, J.-L. Liu and X.-S. Li, *Catal. Today*, 2019, **337**, 69–75.

130 D. H. Choi, D. Han, S. Shim and S. Y. Moon, *Curr. Appl. Phys.*, 2025, **75**, 8–14.

131 R. Garcia-Villalva, M. Biset-Peiró, A. Alarcón, C. Bacariza, S. Murcia-López and J. Guilera, *Int. J. Hydrogen Energy*, 2024, **59**, 1367–1375.

132 Q. Lu, Y. Hou, S. R. Laraib, O. Khalifa, K. Li, W.-L. Xie, M.-S. Cui and Y.-P. Yang, *Fuel Process. Technol.*, 2019, **192**, 57–64.

133 X. Zhao, T. Chen, Y. Wang, K. Li, R. Zhan and H. Lin, *Chem. Eng. J.*, 2023, **457**, 141126.

134 K. Oshima, T. Shinagawa, M. Haraguchi and Y. Sekine, *Int. J. Hydrogen Energy*, 2013, **38**, 3003–3011.

135 Y. R. Lu and P. A. Nikrityuk, *Fuel*, 2022, **319**, 123596.

136 B. Tan, Y. Ye, Z. Huang, L. Ye, M. Ma and Y. Zhou, *Chin. Chem. Lett.*, 2020, **31**, 1530–1534.

137 Y. Cho, A. Yamaguchi and M. Miyauchi, *Catalysts*, 2020, **11**, 18.

138 K. Shimura, H. Kawai, T. Yoshida and H. Yoshida, *Chem. Commun.*, 2011, **47**, 8958–8960.

139 B. Han, W. Wei, M. Li, K. Sun and Y. H. Hu, *Chem. Commun.*, 2019, **55**, 7816–7819.

140 K. Zhao, L. Li, A. Zheng, Z. Huang, F. He, Y. Shen, G. Wei, H. Li and Z. Zhao, *Appl. Energy*, 2017, **197**, 393–404.

141 A. N. Antzaras, E. Heracleous and A. A. Lemonidou, *Fuel Process. Technol.*, 2020, **208**, 106513.

142 T. Papalas, A. N. Antzaras and A. A. Lemonidou, *Appl. Catal., B*, 2024, **347**, 123777.

143 Y. Yang, Y. Qiu, Z. Zhang, S. Wang, H. Chen, D. Zeng and R. Xiao, *Energy Fuels*, 2023, **37**, 12788–12795.

144 Z. Hu, Z. Miao, J. Wu and E. Jiang, *Int. J. Hydrogen Energy*, 2021, **46**, 39700–39718.

145 Y. Zheng, L. Zhao, Y. Wang, Y. Wang, H. Wang, Y. Wang, L. Jiang, X. Zhu, Y. Wei and K. Li, *Fuel Process. Technol.*, 2021, **215**, 106744.

146 X. Yin, S. Wang, B. Wang and L. Shen, *Chem. Eng. J.*, 2021, **422**, 128751.

147 X. Yin, S. Wang, B. Wang and L. Shen, *Chem. Eng. J.*, 2021, **422**, 128751.

148 J. Wang, L. Shen, L. Wang and B. Sundén, *Chem. Eng. Sci.*, 2024, **295**, 120157.

1976 | *React. Chem. Eng.*, 2025, **10**, 1963–1977

This journal is © The Royal Society of Chemistry 2025

149 W.-J. Sheu, Z.-W. Hsu, W.-H. Chen and Y.-C. Chen, *Int. J. Hydrogen Energy*, 2024, **52**, 938–952.

150 F. Alrashed and U. Zahid, *Comput. Chem. Eng.*, 2021, **154**, 107497.

151 M. A. Habib, A. Harale, S. Paglieri, F. S. Alrashed, A. Al-Sayoud, M. V. Rao, M. A. Nemitallah, S. Hossain, M. Hussien, A. Ali, M. A. Haque, A. Abuelyamen, M. R. Shakeel, E. M. A. Mokheimer and R. Ben-Mansour, *Energy Fuels*, 2021, **35**, 5558–5593.

152 M. A. Nemitallah, *Case Stud. Therm. Eng.*, 2023, **45**, 102939.

153 M. Wang, X. Tan, J. Motuzas, J. Li and S. Liu, *J. Membr. Sci.*, 2021, **620**, 118909.

154 L. Fan, C. E. Li, P. V. Aravind, W. Cai, M. Han and N. Brandon, *J. Power Sources*, 2022, **538**, 231573.

155 L. Fan, C. E. Li, L. van Biert, S.-H. Zhou, A. N. Tabish, A. Mokhov, P. V. Aravind and W. Cai, *Renewable Sustainable Energy Rev.*, 2022, **166**, 112646.

156 N. Shi, Y. Xie, Y. Yang, S. Xue, X. Li, K. Zhu, D. Huan, R. Peng, C. Xia and Y. Lu, *Mater. Renewable Sustainable Energy*, 2020, **9**, 1–18.

157 Y. Yang, Y. Liu, Z. Chen, M. Li, M. Rao, X. Wang, P. Feng, F. Zhou and Y. Ling, *Sep. Purif. Technol.*, 2022, **288**, 120665.

158 B. Tu, X. Su, Y. Yin, F. Zhang, X. Lv and M. Cheng, *Fuel*, 2020, **278**, 118273.

159 S. Vecino-Mantilla, P. Gauthier-Maradei, M. Huvé, J. M. Serra, P. Roussel and G. H. Gauthier, *ChemCatChem*, 2019, **11**, 4631–4641.

160 W. Zhang, F. Yin, Z. Cheng, S. Peng and C. Sun, *Fuel*, 2023, **354**, 129356.

This journal is © The Royal Society of Chemistry 2025

React. Chem. Eng., 2025, **10**, 1963–1977 | **1977**